AGU PUBLICATIONS

Geophysical Research Letters

RESEARCH LETTER
10.1002/2015GL064892

Key Points:
- The LIDAR on the Phoenix Mars mission observed detached layers of dust
- For the first time, such layers are simulated in a general circulation model
- The layers continue to rise above the surface boundary layer by solar heating

Supporting Information:
- Supporting Information S1
- Movie S1
- Movie S2

Correspondence to:
F. Daerden,
Frank.Daerden@aeronomie.be

Citation:
Daerden, F., J. A. Whiteway, L. Neary, L. Komguem, M. T. Lemmon, N. G. Heavens, B. A. Cantor, E. Hébrard, and M. D. Smith (2015), A solar escalator on Mars: Self-lifting of dust layers by radiative heating, *Geophys. Res. Lett.*, *42*, doi:10.1002/2015GL064892.

Received 29 JUN 2015
Accepted 23 AUG 2015
Accepted article online 27 AUG 2015

A solar escalator on Mars: Self-lifting of dust layers by radiative heating

F. Daerden[1], J. A. Whiteway[2], L. Neary[1], L. Komguem[2], M. T. Lemmon[3], N. G. Heavens[4], B. A. Cantor[5], E. Hébrard[6,7], and M. D. Smith[6]

[1]Belgian Institute for Space Aeronomy, Brussels, Belgium, [2]Centre for Research in Earth and Space Science, York University, Toronto, Ontario, Canada, [3]Atmospheric Sciences Department, Texas A&M University, College Station, Texas, USA, [4]Department of Atmospheric and Planetary Sciences, Hampton University, Hampton, Virginia, USA, [5]Malin Space Science Systems, San Diego, California, USA, [6]NASA Goddard Space Flight Center, Greenbelt, Maryland, USA, [7]NASA Postdoctoral Program, Oak Ridge Associated Universities, Oak Ridge, Tennessee, USA

Abstract Dust layers detected in the atmosphere of Mars by the light detection and ranging (LIDAR) instrument on the Phoenix Mars mission are explained using an atmospheric general circulation model. The layers were traced back to observed dust storm activity near the edge of the north polar ice cap where simulated surface winds exceeded the threshold for dust lifting by saltation. Heating of the atmospheric dust by solar radiation caused buoyant instability and mixing across the top of the planetary boundary layer (PBL). Differential advection by wind shear created detached dust layers above the PBL that ascended due to radiative heating and arrived at the Phoenix site at heights corresponding to the LIDAR observations. The self-lifting of the dust layers is similar to the "solar escalator" mechanism for aerosol layers in the Earth's stratosphere.

1. Introduction

Laser remote sensing measurements of the vertical distribution of dust in the atmosphere of Mars [*Whiteway et al.*, 2008, 2009; *Komguem et al.*, 2013] above the landing site of the NASA Phoenix mission [*Smith et al.*, 2008, 2009] were nearly identical to similar measurements above the Australian desert within the planetary boundary layer (PBL). The PBL depth was about 4 km in each case [*Dickinson et al.*, 2011]. The similarity does not extend to heights above the top of the PBL, where dust is a dominant constituent in the atmosphere of Mars but not on Earth. On Mars the dust content is reduced above the PBL but continues to be approximately well mixed and proportional to atmospheric pressure up to heights above 20 km [*Heavens et al.*, 2011; *Komguem et al.*, 2013]. The mechanisms for transporting dust from the surface to heights above the PBL on Mars are the subject of this report.

For the atmosphere of the Earth, it has been shown that radiative heating will result in self-lifting of layers containing particulate material, such that the aerosol plays an active role in its vertical transport [*Boers et al.*, 2010; *de Laat et al.*, 2012]. This has been observed in the stratosphere and referred to as a "solar escalator" since vertical steps in dust layers correspond to the diurnal cycle in solar radiative heating [*de Laat et al.*, 2012]. The radiative heating of dust has also been recognized as being potentially more significant in the atmosphere of Mars [*Fuerstenau*, 2006; *Heavens et al.*, 2011; *Spiga et al.*, 2013] since the molecular density there is a factor of 100 less than on Earth. In this study a general circulation model of the atmosphere on Mars was used to explain the observation of dust layers that were decoupled from the PBL. It was found that the radiative self-lifting process was playing a substantial role in the vertical transport and that the solar escalator analogy is also applicable on Mars.

2. Measurements

The LIDAR instrument on the NASA Phoenix Mars mission provided vertical profile measurements of atmospheric dust [*Dickinson et al.*, 2011; *Komguem et al.*, 2013] and water ice clouds [*Whiteway et al.*, 2009; *Dickinson et al.*, 2010] above the northern high-latitude landing site (68.2°N, 125.7°W) over a period from late spring to late summer (aerocentric longitudes, L_s, of 76.6° to 151°). The optical extinction coefficient was derived from the LIDAR measurements, and this was used as an indicator of the amount of dust loading. Around summer solstice ($L_s = 90°$) the measured optical extinction coefficient was enhanced within the

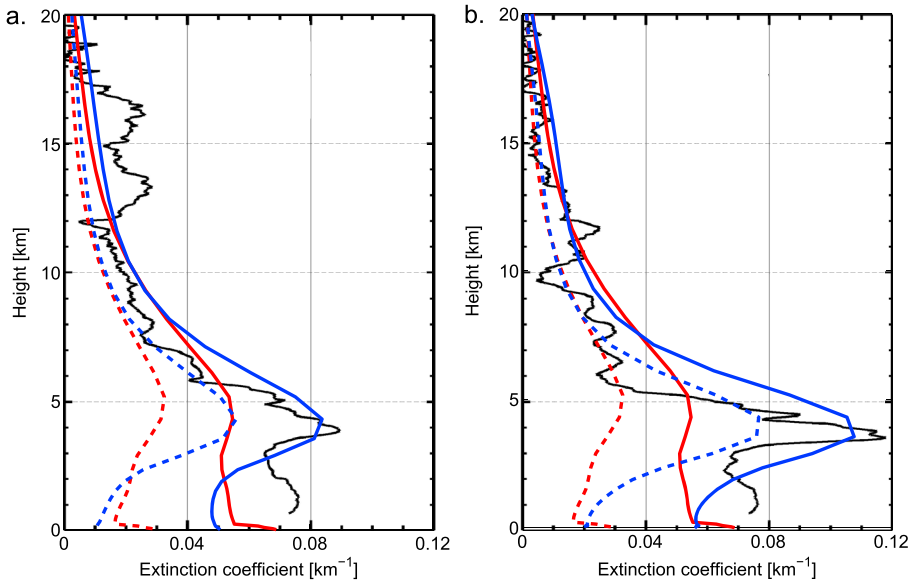

Figure 1. Vertical profiles of optical extinction coefficient at wavelength 532 nm derived from the Phoenix LIDAR measurements (solid black lines) showing separated dust layers peaking at height 4 km on mission sols (a) 20 (L_s = 85.6°) and (b) 30 (L_s = 90°). The measurement uncertainty was ±0.005 km^{-1} at a height of 4 km and increased gradually with height to ±0.007 km^{-1} at a height of 10 km. The vertical profile of optical extinction coefficient from the model simulation is shown above the Phoenix site at L_s = 91.8 (red). The blue lines are the simulated extinction coefficient profiles selected along a back trajectory starting at L_s = 91.8 at height 5 km over the Phoenix site, for L_s = 90° in Figure 1a and 89° in Figure 1b. The back trajectory and the positions of these profiles are indicated in Figures 3 and 4. Full lines represent total extinction and dashed lines the portion due to wind lifting.

well-mixed PBL [*Komguem et al.*, 2013]. There were also distinct layers of material observed at and above the top of the PBL (heights 4–7 km) around summer solstice. In the present paper we focus on two cases with a layer at height 4 km (Figure 1).

These layers are considered to be dust rather than water ice clouds since they were observed during the warmest part of the day (afternoon) as well as at night. Later in the summer the LIDAR detected clouds at the PBL top but only in the early morning hours when the temperature would drop below the water frost point of about −62° C [*Whiteway et al.*, 2009]. This was confirmed with simulations [*Daerden et al.*, 2010]. Clouds could not form at height 4 km during the afternoon at summer solstice unless the amount of water vapor in the PBL was much greater than the amount measured at the surface on the Phoenix lander. Also, there was no ground ice fog observed around summer solstice when the surface temperatures at night where much lower than at the top of the PBL. Ground ice fog was observed by the LIDAR only later in the summer, 40 Martian solar days (sols) after solstice [*Dickinson et al.*, 2010]. Until now there has been no explanation for the layers at the top of the PBL at summer solstice.

3. Model

A general circulation model for the atmosphere of Mars was developed and applied here for interpreting measurements of dust from the NASA Phoenix mission. It was based on the Canadian Global Environmental Multiscale (GEM) model for weather forecasting on Earth [*Côté et al.*, 1998; *Moudden and McConnell*, 2005; *Akingunola*, 2008]. The model was operated on a grid with a horizontal resolution of 4° × 4° and with 102 hybrid vertical levels reaching from the surface to ~150 km. The vertical resolution was 35 m near the surface and increased gradually to ~1.2 km at height 10 km. At the latitude of the Phoenix landing site, the PBL was resolved with 17 vertical layers. The integration timestep was 1/48 of a sol.

Processes added to the model for the present study include dust with radiative transfer using the refractive index of *Wolff et al.* [2006, 2009] as in *Madeleine et al.* [2011], carbon dioxide with surface exchange [*Forget et al.*, 1998],

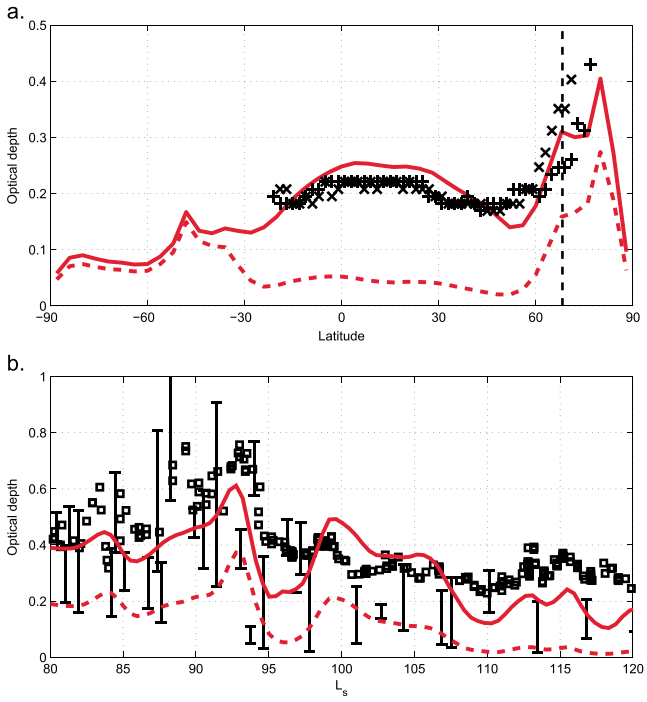

Figure 2. (a) The latitudinal distribution of zonally averaged dust optical depths at 991 nm from the simulation, scaled to the 6.1 mbar pressure level and averaged over the period $L_s = 89°–91°$ (full red line). The dashed line represents the portion of the simulated dust due to wind lifting. The black data points are the optical depths measured from orbit by the TES instrument, scaled to 6.1 mbar, averaged zonally and over the period $L_s = 89°–91°$ in Mars years 25 (+) and 26 (x). The absorption optical depths from TES were transformed to extinction optical depths using a factor of 1.3 [*Smith*, 2004] and scaled from 9.3 μm to visible wavelengths using a factor of 2 [*Clancy et al*., 2003]. Only data with a surface temperature of 238 K or higher were retained in the plot in order to reduce uncertainties in the vicinity of the polar ice caps. The vertical black dashed line indicates the latitude of the Phoenix Lander. (b) Time series of the total daytime optical depth measured by the Phoenix SSI instrument at wavelength 991 nm (black) compared with the simulation result at the Phoenix site (red full line). Also indicated is the portion of the simulated dust optical depth that originated from the wind lifting near the polar cap (red dashed line). The error bars represent the range in optical depth measurements by TES in Mars years 25 and 26 within 2° longitude and 2° latitude of the Phoenix site. The TES data have been scaled to visible extinction optical depths as in Figure 1a.

a multilayered thermal soil model [*Savijärvi*, 1992], turbulent transport in the atmospheric surface layer based on Monin-Obhukov similarity theory [*Louis*, 1979; *Pielke*, 1990], convective transport inside the PBL following *Holtslag and Boville* [1993] (without the countergradient term), and the effects of topography with a low level blocking scheme including gravity wave drag [*Zadra et al*., 2003]. The geophysical boundary conditions include topography [*Smith et al*., 1999], albedo [*Christensen et al*., 2001], thermal inertia [*Putzig et al*., 2005], and roughness length [*Hébrard et al*., 2012]. The recommendations of *Haberle et al*. [2006] for polar cap emissivity and albedo were followed. The depth of the subsurface ice table was set in accordance with *Mellon et al*. [2004].

Dust lifting processes were implemented in the model following *Kahre et al*. [2006]. The dust particle size distribution was represented with three size bins (0.1, 1.5, and 10 μm). Dust was lifted from the surface by saltation [*Kok et al*., 2012] following the "Kahre-Murphy-Haberle (KMH)" method [*Kahre et al*., 2006] when the surface wind stress exceeded a threshold value of 0.0225 Pa [*Haberle et al*., 2003]. A detailed roughness length map was applied [*Hébrard et al*., 2012], and the mean value of roughness length inside every grid cell was used. The efficiency factor for wind lifting was set to 0.15. The dust mass flux from small-scale vortices (dust devils, *Kok et al*. [2012]) was proportional to the surface turbulent heat flux and the height of the PBL [*Renno et al*., 1998]. The efficiency factor for the dust devil mass flux was set to 6×10^{-9} kg/J. Sedimentation of the dust particles was taken into account using the Stokes settling velocity with Cunningham slip-flow correction [*Pruppacher and Klett*, 1997]. These settings allowed the model to reproduce the latitude distribution of dust as observed by the Thermal Emission Spectrometer (TES) instrument [*Smith*, 2004] on the NASA Mars Global Surveyor (MGS) mission at northern summer solstice (Figure 2a).

At high northern latitudes the large optical depths measured by TES from orbit (Figure 2a) and by the Surface Stereo Imager (SSI) instrument on Phoenix [*Tamppari et al*., 2010] (Figure 2b) could only be reproduced by including wind gusting at latitudes north of 60°N. Also, the dust devil efficiency factor had to be increased to 3.0×10^{-8} kg/J at these latitudes. A subgrid-scale treatment of the roughness map was also implemented north of 60°N latitude but did not lead to a significant increase in dust optical depths. Wind gusting was incorporated in the model using a Weibull distribution (see, e.g., *Newman et al*. [2002]), assuming that the model winds are the averaged values of the distribution. The resulting dust mass flux was then computed as in *Newman et al*. [2002]. A Weibull shape factor of unity resulted in a dust optical depth that was in agreement

with the measurements (Figure 2). The different settings for dust lifting at latitudes north of 60°N reflect the fact that dust lifting parameters that lead to a simulation that matches the dust loading at low latitudes do not produce sufficient dustiness at high northern latitudes. This could be explained by the presence of a strong dust source such as the extended dune fields in the north polar region [*Cutts et al*., 1976] and the sublimation lag from the evaporating seasonal polar ice cap. Another factor is that the model's resolution may not sufficiently allow for a detailed enough prescription of the permanent polar cap and related high friction velocities over ice-soil boundaries.

Where heating of airborne dust by absorption of solar radiation created regions of convective instability in the model, the temperature, momentum, and constituents (including dust) were vertically mixed over the unstable model levels in order to regain stability. Inside the PBL the implemented convective diffusion parameterization [*Holtslag and Boville*, 1993] provided the required mixing. Above the PBL, the vertical mixing was simulated with a parameterization of eddy diffusion [*Holtslag and Boville*, 1993], in which the eddy diffusion coefficients were calculated using a mixing length and a stability function based on the gradient flux Richardson number. The form of the stability function was chosen as in *Haberle et al*. [1999], and the mixing length was set to 500 m.

4. Simulations

The model simulations were validated by comparing with various data sets. The annual cycle of CO_2 ice mass in the polar caps in the simulation was in agreement with the observations by the gamma ray spectrometer on the NASA Mars Odyssey mission [*Kelly et al*., 2006]. The latitudinal distribution of dust optical depth around solstice was in agreement with measurements from TES (Figure 2a). The simulated surface atmospheric pressure cycle was in agreement with the measurements on the NASA Viking Lander 1 [*Hess et al*., 1976] and the NASA Phoenix [*Taylor et al*., 2010] missions. The diurnal range in the simulated temperature at a height of 2 m at the Phoenix lander site was in agreement with measurements on the Phoenix Lander [*Davy et al*., 2010]. The simulated PBL depth was in agreement with the Phoenix LIDAR measurements [*Komguem et al*., 2013].

The model simulation of the vertical profile of the optical extinction coefficient of dust was verified by comparison with measurements from the Mars Climate Sounder (MCS) instrument on the Mars Reconnaissance Orbiter (MRO) mission [*McCleese et al*., 2007; *Kleinböhl et al*., 2009; *Heavens et al*., 2011] at the time of the Phoenix mission and with measurements from the LIDAR instrument on the Phoenix Lander. Some selected cases are shown in Figures S1a, S1b, and S1c in the supporting information. The optical extinction coefficient was retrieved from MCS measurements at wavelength 21 μm and then scaled using a multiplicative factor of 7.3 [*Kleinböhl et al*., 2011] in order to compare at the wavelength of 532 nm used by the Phoenix LIDAR. When there was overlap in the height of the measurements, the LIDAR and MCS dust extinction coefficient profiles matched within the measurement uncertainty. The simulated vertical profiles of dust optical extinction coefficient were found to be within the range of variability and measurement uncertainty in the observations (Figures S1a, S1b, and S1c). The simulated vertical profile of temperature was also compared with measurements from MCS above the Phoenix site at the time of the mission. The simulations and measurements were in agreement within natural variability, and one example is provided in the supporting information (Figure S1d).

The simulations were also in agreement with the variation in the total atmospheric optical depth as observed by the SSI instrument on the Phoenix lander over the period around summer solstice when the dust loading was a maximum (Figure 2b) [*Tamppari et al*., 2010]. A peak in optical depth just after summer solstice in the simulation was due to transport of dust that was originally lifted by saltation at the edge of the polar ice cap and then transported to the Phoenix site (Figure 3a). This was found to be an annually repeating phenomenon when the model was run for several Mars years since the timing was linked to the retreat of the seasonal CO_2 ice cap to within the north polar sand sea (the dark albedo area surrounding the polar cap in Figure 3b). At this point the albedo contrast between the cap and surrounding soil was maximal, leading to sharp thermal gradients, causing strong near-surface winds, and dust lifting by saltation. The area of dust lifting in the simulation roughly coincided with a large dust cloud observed from orbit by the Mars Color Imager (MARCI) instrument [*Cantor et al*., 2010] on the NASA MRO mission (Figure 3b) that started at L_s~85° at the edge of the cap at longitude ~90°W. A sequence of MARCI images shows that dust was arising from this event and was spreading out toward southern latitudes and in the eastern direction (Movie S1). The simulation shows a similar evolution (Movie S2).

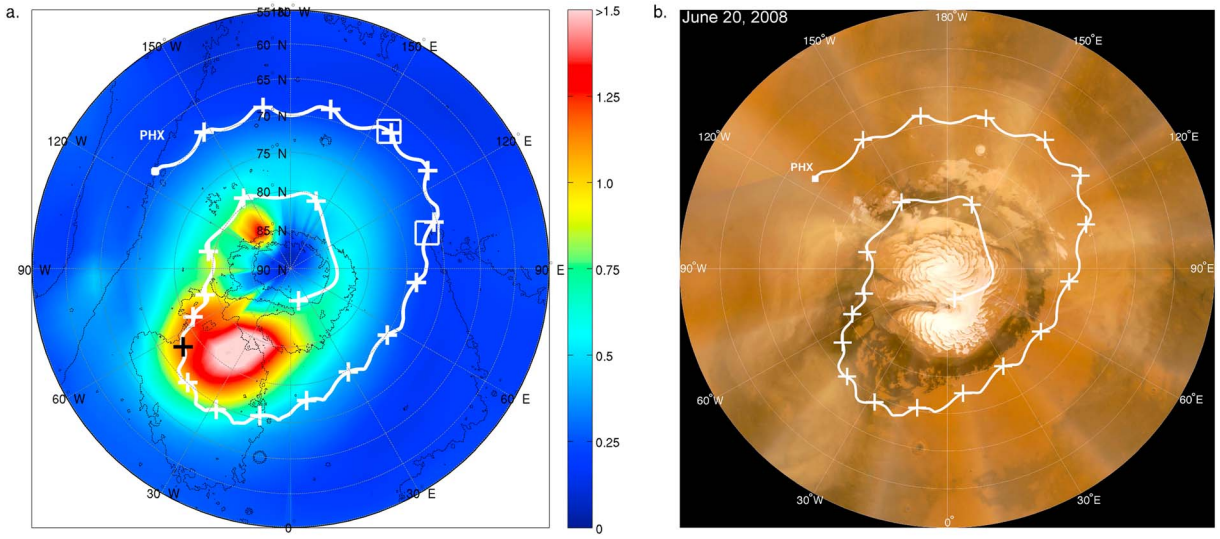

Figure 3. (a) Map of simulated dust optical depth at wavelength 991 nm at L_s=85°. The white line is a 20-sol back trajectory starting from the Phoenix site at height 5 km at L_s=91.8°, the time of the simulated detached layer plotted in red in Figure 1. The markers on the back trajectory have a spacing of 1 sol. The location of the back trajectory at the time of the map is indicated by a black cross (+). The locations of the extinction profiles plotted in blue in Figure 1 are indicated by squares. (b) Mosaic image from MARCI images on June 20, 2008 (L_s=88)°, with a dust cloud visible at longitudes 30°-120°W. The simulated back trajectory from Phoenix is overlaid and passes through this observed dust cloud.

The model wind fields were used to calculate a back trajectory from a detached layer that was simulated above the PBL at the Phoenix site around solstice (Figure 1). Going back 12 to 16 sols, the air passed through a region of enhanced dust abundance originating from strong wind-lifting events close to the polar cap (Figure 3a). By a combination of radiative heating, mixing due to convective instability, and resolved atmospheric circulation (advection), the lifted dust had spread out to latitudes around 75°N where the back trajectory from Phoenix passed.

A crucial aspect of the simulations was heating of the dust by absorption of solar radiation. At the high latitudes of the polar cap edge the PBL is relatively shallow, and any dust that gets lifted there would mix only up to a few 100 m by the surface layer turbulent mixing. The atmospheric dust was heated by solar radiation which, averaged over a day, was stronger than the IR radiative cooling. This drove two mechanisms for vertical transport. The first was that the temperature response of the atmosphere caused convective instability that triggered turbulent mixing in the model and transport of dust to heights above the PBL. The other mechanism of vertical transport was self-lifting of dust layers due to solar heating.

An explanation for the separated layers of dust observed by the Phoenix LIDAR is provided by plotting the contour of the vertical profile of dust optical extinction coefficient along the back trajectory (Figure 4a). Moving forward in time (from the left side of Figure 4a), the dust was mixed above the PBL starting at $L_s = 85°$, when the trajectory passed over the ice-soil boundary and there was a marked enhancement in dust lifting. As the wind speed increased with height above the ground, the dust was first advected further downwind at greater heights. After $L_s = 88.5°$ the differential advection by wind shear produced a separated dust layer with the trajectory at height 2.7 km. The trajectory continued to rise to height 5 km before it arrived above the Phoenix site at $L_s = 91.8°$. The gradual lifting of the dust layer after $L_s = 88.5°$ was caused by the radiative heating of the dust, which is plotted along the back trajectory in Figure 4b. The ascent of the trajectory caused by heating due to solar radiation during daytime exceeded the descent caused by cooling due to IR radiation at night. The diurnal cycle in radiative heating and cooling caused a step-like trajectory after $L_s = 88.5°$ in Figure 4. The radiative heating resulted in a vertical displacement of the dust layer to an altitude where the increased potential temperature matched that of the environment. In the time period between when the layer became detached from the PBL ($L_s \sim 88.5°$) and when the time when the layer passed over the Phoenix site ($L_s = 91.8°$), the integrated heating along the trajectory was 45 K in terms of potential temperature (red line in Figure 4c). This was slightly greater than the change in potential temperature in the background atmosphere between heights of 2.7 and 5 km, corresponding to the vertical displacement of the layer

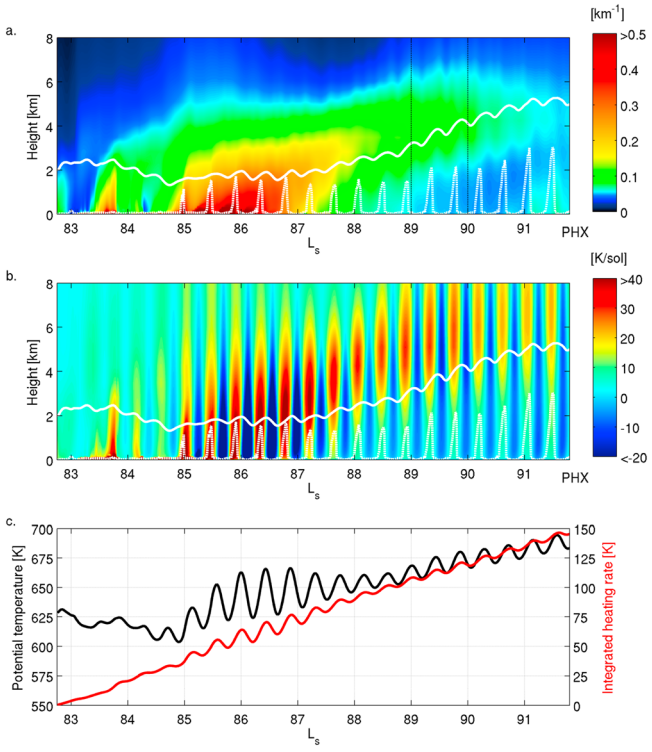

Figure 4. (a) Contour plot of the vertical profile of the simulated dust extinction coefficient at wavelength 532 nm along the back trajectory of Figure 3. The right hand edge corresponds to the situation at Phoenix at $L_s = 91.8°$, i.e., the simulated profile plotted in red in Figure 1. The full white line represents the height of the trajectory shown in Figure 3. The dashed white line represents the height of the top of the simulated planetary boundary layer. The vertical black dashed lines indicate the times of the extinction profiles plotted in blue in Figure 1. (b) Simulated net (solar + IR) dust heating rate along the back trajectory, in K/sol (solar day). (c) The potential temperature of the parcel of air followed along the back trajectory (black line) and the integrated heating rate along the trajectory (red).

(black line in Figure 4c). The difference was due to mixing. A significant factor was that the sunlight was incident for an entire sol (solar day) at the latitude of the dust layer during midsummer, and offset the IR radiative cooling at night. The mechanism for self-lifting by radiative heating and the resulting step-like trajectory is similar to what has been referred to as the "solar escalator" for aerosol layers in the stratosphere of the Earth [*de Laat et al.*, 2012].

The vertical profile of dust extinction coefficient from the simulation at $L_s = 91.8°$ is compared to the Phoenix LIDAR observations in Figure 1 (red line). The model simulation results in a layer of enhanced dust at heights 4–5 km that corresponds to the observations. Going back along the back trajectory, the simulated extinction profiles shown in Figure 1 from $L_s = 90°$ and 89° (blue lines) have even closer similarity to the measured profiles. The model reproduces the LIDAR measurements within the same latitude range.

5. Conclusions

A general circulation model for the atmosphere of Mars has been applied to explain dust layers that were observed by the LIDAR instrument on the Phoenix mission. The present paper focuses on dust layers that were observed at 4 km height around solstice. In the simulation the dust was lifted from the surface near the edge of the polar cap where strong winds were driven by the thermal gradients associated with the albedo contrast between bare land and ice. Heating due to absorption of solar radiation caused mixing of the dust to heights above the PBL where differential advection by shear drew the dust out into a layer. Heating of the layer by absorption of solar radiation then caused it to ascend further into the troposphere above the PBL. A similar process has been observed to occur in the stratosphere of the Earth, and it has been called the solar escalator [*de Laat et al.*, 2012]. This study provides evidence that the solar escalator mechanism can contribute to the sustenance of dust in the atmosphere of Mars at heights above the PBL.

Acknowledgments

The model output used in this paper is available by request from author Daerden. The LIDAR, SSI, and MCS data used in this paper are freely available on the NASA Planetary Data System. The MARCI images used in this paper are available by request from author Cantor. This research was carried out with support from the Belgian Federal Science Policy Office (BELSPO) under grant MO/35/029 and from the Space Science Enhancement Program of the Canadian Space Agency (CSA). Support for the LIDAR instrument Science Team during the Phoenix mission was provided by the CSA under contract 9F007-070437/001/SR. The Phoenix mission was led by Peter H. Smith at the University of Arizona, on behalf of NASA, and managed by the Jet Propulsion Laboratory.

The Editor thanks Robert Wilson and Aymeric Spiga for their assistance in evaluating this paper.

References

Akingunola, A. (2008), Martian water cycle modeling with the second generation of the global Mars multiscale model, PhD thesis, York Univ., Toronto, Canada.

Boers, R., A. T. de Laat, D. C. Stein Zweers, and R. J. Dirksen (2010), Lifting potential of solar-heated aerosol layers, *Geophys. Res. Lett.*, *37*, L24802, doi:10.1029/2010GL045171.

Cantor, B. A., P. B. James, and W. M. Calvin (2010), MARCI and MOC observations of the atmosphere and surface cap in the north polar region of Mars, *Icarus*, *208*, 61–81, doi:10.1016/j.icarus.2010.01.032.

Christensen, P. R., et al. (2001), Mars Global Surveyor Thermal Emission Spectrometer experiment: Investigation description and surface science results, *J. Geophys. Res.*, *106*, 23,823–23,871, doi:10.1029/2000JE001370.

Clancy, R. T., M. J. Wolff, and P. R. Christensen (2003), Mars aerosol studies with the MGS TES emission phase function observations: Optical depths, particle sizes, and ice cloud types versus latitude and solar longitude, *J. Geophys. Res.*, *108*(E9), 5098, doi:10.1029/2003JE002058.

Côté, J., S. Gravel, A. Méthot, A. Patoine, M. Roch, and A. Staniforth (1998), The operational CMC–MRB global environmental multiscale (GEM) model. Part I: Design considerations and formulation, *Mon. Weather Rev.*, *126*, 1373–1395.
Cutts, J. A., K. R. Blasius, G. A. Briggs, M. H. Carr, R. Greeley, and H. Masursky (1976), North polar region of Mars: Imaging results from viking 2, *Science*, *194*(4271), 1329–1337, doi:10.1126/science.194.4271.1329.
Daerden, F., J. A. Whiteway, R. Davy, C. Verhoeven, L. Komguem, C. Dickinson, P. A. Taylor, and N. Larsen (2010), Simulating observed boundary layer clouds on Mars, *Geophys. Res. Lett.*, *37*, L04203, doi:10.1029/2009GL041523.
Davy, R., J. A. Davis, P. A. Taylor, C. F. Lange, W. Weng, J. Whiteway, and H. P. Gunnlaugson (2010), Initial analysis of air temperature and related data from the Phoenix MET station and their use in estimating turbulent heat fluxes, *J. Geophys. Res.*, *115*, E00E13, doi:10.1029/2009JE003444.
de Laat, A. T. J., D. C. Stein Zweers, R. Boers, and O. N. E. Tuinder (2012), A solar escalator: Observational evidence of the self-lifting of smoke and aerosols by absorption of solar radiation in the February 2009 Australian Black Saturday plume, *J. Geophys. Res.*, *117*, D04204, doi:10.1029/2011JD017016.
Dickinson, C., J. A. Whiteway, L. Komguem, J. E. Moores, and M. T. Lemmon (2010), Lidar measurements of clouds in the planetary boundary layer on Mars, *Geophys. Res. Lett.*, *37*, L18203, doi:10.1029/2010GL044317.
Dickinson, C., L. Komguem, J. A. Whiteway, M. Illnicki, V. Popovici, W. Junkermann, P. Connolly, and J. Hacker (2011), Lidar atmospheric measurements on Mars and Earth, *Planet. Space Sci.*, *59*, 942–951, doi:10.1016/j.pss.2010.03.004.
Forget, F., F. Hourdin, R. Fournier, C. Hourdin, O. Talagrand, M. Colins, S. R. Lewis, P. L. Read, and J. P. Huot (1998), CO_2 snowfall on mars: Simulation with a general circulation model, *Icarus*, *131*, 302–316.
Fuerstenau, S. D. (2006), Solar heating of suspended particles and the dynamics of Martian dust devils, *Geophys. Res. Lett.*, *33*, L19S03, doi:10.1029/2006GL026798.
Haberle, R. M., et al. (1999), General circulation model simulations of the Mars Pathfinder atmospheric structure investigation/meteorology data, *J. Geophys. Res.*, *104*, 8957–8974, doi:10.1029/1998JE900040.
Haberle, R. M., J. R. Murphy, and J. Schaeffer (2003), Orbital change experiments with a Mars general circulation model, *Icarus*, *161*, 66.
Haberle, R. M., F. Forget, A. Colaprete, J. Schaeffer, W. V. Boynton, N. J. Kelly, and M. A. Chamberlain (2006), The effect of ground ice on the Martian seasonal CO_2 cycle, *Planet. Space Sci.*, *56*, 251–255, doi:10.1016/j.pss.2007.08.006.
Heavens, N. G., M. I. Richardson, A. Kleinböhl, D. M. Kass, D. J. McCleese, W. Abdou, J. L. Benson, J. T. Schofield, J. H. Shirley, and P. M. Wolkenberg (2011), Vertical distribution of dust in the Martian atmosphere during northern spring and summer: High-altitude tropical dust maximum at northern summer solstice, *J. Geophys. Res.*, *116*, E01007, doi:10.1029/2010JE003692.
Hébrard, E., C. Listowski, P. Coll, B. Marticorena, G. Bergametti, A. Määttänen, F. Montmessin, and F. Forget (2012), An aerodynamic roughness length map derived from extended Martian rock abundance data, *J. Geophys. Res.*, *117*, E04008, doi:10.1029/2011JE003942.
Hess, S. L., et al. (1976), Preliminary meteorological results on Mars from the Viking 1 lander, *Science*, *193*, 788–791.
Holtslag, A. A. M., and B. A. Boville (1993), Local versus nonlocal boundary-layer diffusion in a global climate model, *J. Clim.*, *6*, 1825–1842.
Kahre, M. A., J. R. Murphy, and R. M. Haberle (2006), Modeling the Martian dust cycle and surface dust reservoirs with the NASA Ames general circulation model, *J. Geophys. Res.*, *111*, E06008, doi:10.1029/2005JE002588.
Kelly, N. J., W. V. Boynton, K. Kerry, D. Hamara, D. Janes, R. C. Reedy, K. J. Kim, and R. M. Haberle (2006), Seasonal polar carbon dioxide frost on Mars: CO_2 mass and columnar thickness distribution, *J. Geophys. Res.*, *111*, E03S07, doi:10.1029/2006JE002678.
Kleinböhl, A., et al. (2009), Mars Climate Sounder limb profile retrieval of atmospheric temperature, pressure, and dust and water ice opacity, *J. Geophys. Res.*, *114*, E10006, doi:10.1029/2009JE003358.
Kleinböhl, A., J. T. Schofield, W. A. Abdou, P. G. J. Irwin, and R. J. de Kok (2011), A single-scattering approximation for infrared radiative transfer in limb geometry in the Martian atmosphere, *J. Quant. Spectrosc. Radiat. Transfer*, *112*, 1568–1580, doi:10.1016/j.jqsrt.2011.03.006.
Kok, J. F., E. J. R. Parteli, T. I. Michaels, and D. Bou Karam (2012), The physics of wind-blown sand and dust, *Rep. Prog. Phys.*, *75*, 106901, doi:10.1088/0034-4885/75/10/106901.
Komguem, L., J. A. Whiteway, C. Dickinson, M. Daly, and M. T. Lemmon (2013), Phoenix LIDAR measurements of Mars atmospheric dust, *Icarus*, *223*, 649–653, doi:10.1016/j.icarus.2013.01.020.
Louis, J. F. (1979), A parametric model of vertical eddy fluxes in the atmosphere, *Boundary Layer Meteorol.*, *17*, 187–202.
Madeleine, J.-. B., F. Forget, E. Millour, L. Montabone, and M. J. Wolff (2011), Revisiting the radiative impact of dust on Mars using the LMD Global Climate Model, *J. Geophys. Res.*, *116*, E11010, doi:10.1029/2011JE003855.
McCleese, D. J., J. T. Schofield, F. W. Taylor, S. B. Calcutt, M. C. Foote, D. M. Kass, C. B. Leovy, D. A. Paige, P. L. Read, and R. W. Zurek (2007), Mars Climate Sounder: An investigation of thermal and water vapor structure, dust and condensate distributions in the atmosphere, and energy balance of the polar regions, *J. Geophys. Res.*, *112*, E05S06, doi:10.1029/2006JE002790.
Mellon, M. T., W. C. Feldman, and T. H. Prettyman (2004), The presence and stability of ground ice in the southern hemisphere of Mars, *Icarus*, *169*, 324–340, doi:10.1016/j.icarus.2003.10.022.
Moudden, Y., and J. C. McConnell (2005), A new model for multiscale modeling of the Martian atmosphere, GM3, *J. Geophys. Res.*, *110*, E04001, doi:10.1029/2004JE002354.
Newman, C. E., S. R. Lewis, P. L. Read, and F. Forget (2002), Modeling the Martian dust cycle, 1. Representations of dust transport processes, *J. Geophys. Res.*, *107*(E12), 5123, doi:10.1029/2002JE001910.
Pielke, R. A. (1990), *Mesoscale Meteorological Modeling*, 2nd ed., Academic Press, San Diego, Calif.
Pruppacher, H. R., and J. D. Klett (1997), *Microphysics of Clouds and Precipitation*, 2nd ed., 954 pp., Kluwer Acad., Dordrecht, Netherlands.
Putzig, N. E., M. T. Mellon, K. A. Kretke, and R. E. Arvidson (2005), Global thermal inertia and surface properties of Mars from the MGS mapping mission, *Icarus*, *173*, 325–341, doi:10.1016/j.icarus.2004.08.017.
Renno, N. O., M. L. Burkett, and M. P. Larkin (1998), A simple thermodynamical theory for dust devils, *J. Atmos. Sci.*, *55*, 3244.
Savijärvi, H. (1992), On surface temperature and moisture prediction in atmospheric models, *Contrib. Atmos. Phys.*, *65*, 281–292.
Smith, D. E., et al. (1999), The global topography of Mars and implications for surface evolution, *Science*, *284*, 1495–1503, doi:10.1126/science.284.5419.1495.
Smith, M. D. (2004), Interannual variability in TES atmospheric observations of Mars during 1999–2003, *Icarus*, *167*, 148–165.
Smith, P. H., et al. (2008), Introduction to special section on the Phoenix mission: Landing site characterization experiments, mission overviews, and expected science, *J. Geophys. Res.*, *113*, E00A18, doi:10.1029/2008JE003083.
Smith, P. H., et al. (2009), H_2O at the Phoenix landing site, *Science*, *325*, 58, doi:10.1126/science.1172339.
Spiga, A., J. Faure, J.-B. Madeleine, A. Määttänen, and F. Forget (2013), Rocket dust storms and detached dust layers in the Martian atmosphere, *J. Geophys. Res. Planets*, *118*, 746–767, doi:10.1002/jgre.20046.
Tamppari, L. K., et al. (2010), Phoenix and MRO coordinated atmospheric measurements, *J. Geophys. Res.*, *115*, E00E17, doi:10.1029/2009JE003415.

Taylor, P. A., et al. (2010), On pressure measurement and seasonal pressure variations during the Phoenix mission, *J. Geophys. Res.*, *115*, E00E15, doi:10.1029/2009JE003422.

Whiteway, J. A., M. Daly, A. Carswell, T. Duck, C. Dickinson, L. Komguem, and C. Cook (2008), Lidar on the Phoenix mission to Mars, *J. Geophys. Res.*, *113*, E00A08, doi:10.1029/2007JE003002.

Whiteway, J. A., et al. (2009), Mars water-ice clouds and precipitation, *Science*, *325*, 68–70, doi:10.1126/science.1172344.

Wolff, M. J., et al. (2006), Constraints on dust aerosols from the Mars Exploration Rovers using MGS overflights and Mini-TES, *J. Geophys. Res.*, *111*, E12S17, doi:10.1029/2006JE002786.

Wolff, M. J., M. D. Smith, R. T. Clancy, R. Arvidson, M. Kahre, F. Seelos IV, S. Murchie, and H. Savijärvi (2009), Wavelength dependence of dust aerosol single scattering albedo as observed by the Compact Reconnaissance Imaging Spectrometer, *J. Geophys. Res.*, *114*, E00D04, doi:10.1029/2009JE003350.

Zadra, A., M. Roch, S. Laroche, and M. Charron (2003), The subgrid-scale orographic blocking parametrization of the GEM model, *Atmos. Ocean*, *41*(2), 155–170, doi:10.3137/ao.410204.